# D-4 Nitrogen-Vacancy Centers in Diamond

### From Physics 191r

contributors: M. Lukin, S. Zibrov, M. Goldman (2012)

N-V Centers in Diamond (Sept. 2012 pdf) File:Nvlab 4.pdf

## Contents

# Probing & control of single quantum systems in diamond

## Summary


This experiment explores control over individual quantum objects such as single photons and single electronic spins. It utilizes a confocal microscope to isolate and manipulate individual atom-like impurity in a diamond crystal. Optical excitation of this isolated impurity is used to study a very unusual light source in which single photons are emitted one at a time. Optical and microwave radiation is then used to control and manipulate the electronic spin state associated with the single impurity. Experimental techniques and methods introduced in this experiment form the basis for an exciting modern research direction, involving the applications of individual atoms and atom-like systems for quantum information processing, communication and metrology.


## Learning Goals

- Use a confocal microscope to observe nitrogen-vacancy centers in diamond.
- Measure the correlation function for light emitted by a single n-v center to observe anti-bunching.
- Measure Zeeman splitting of the ground and excited states of an n-v center.
- Observe Rabi oscillations of a single electron.

## Introduction

Control of quantum systems is an important topic in contemporary physics research, with many types of experiments aimed at applications ranging from metrology and interferometry to quantum communication and quantum computation.[1] The key to realization of these concepts and their potential applications is to gain a control over individual quantum systems, such as single photons, atoms, electrons and nuclei. This control should include the ability to prepare and measure such individual degrees of freedom of such systems as well as to manipulate their various degrees of freedom. For example, secure quantum cryptography can be realized by

encoding bits of information into polarization degrees of freedom of individual photons. At the same time, spin degrees of freedom associated with individual electrons can be used as basic building blocks of quantum information processors (quantum bits), or, as an atomic-scale sensors of local fields. [2]

A variety of physical systems lend themselves to such investigations, and each offers a different set of opportunities and challenges. This experiment explores control over individual quantum systems using the so-called Nitrogen-Vacancy impurity in diamond. Such nitrogen-vacancy (NV) centers have been studied for several decades using a variety of spectroscopic techniques. Recently, there has been renewed interest in the NV center as a physical system for quantum information science in the solid state. The NV center is an attractive quantum bit (qubit) candidate because it behaves like an atom trapped in the diamond lattice: it has strong optical transitions, and an electron spin degree of freedom. In what follows we consider the basic structure of the NV center and describe experimental techniques used to probe its spin and optical properties.

# Structure of the NV center

## Physical structure

The NV center is formed by a missing carbon atom adjacent to a substitutional nitrogen impurity in the face-centered cubic (fcc) diamond lattice (see Fig. 1A). The physical structure of this defect -- and the symmetries associated with it -- determine the nature of its electronic states and the dipole-allowed transitions between them (see Fig. 2).

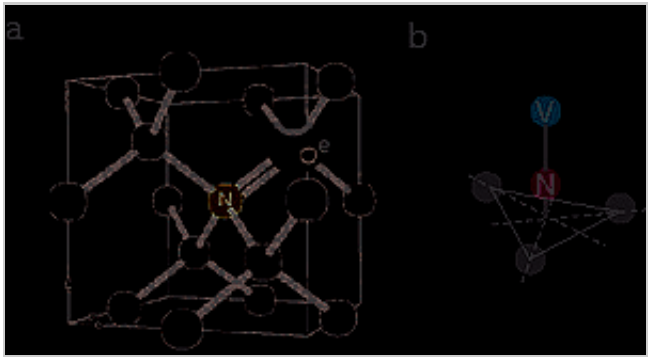


Figure 1. (A) The nitrogen-vacancy center in diamond. (B) The symmetry operations for the $C_{3v}$ group include rotations by $2\pi n$ / 3 around the vertical symmetry axis and reflections in the three planes containing the vertical symmetry axis and one of the nearest-neighbor carbon sites.

The symmetry properties of the NV center provide insight into the nature of its electronic states. Unlike atoms in free space, whose electronic states are governed by their rotational invariance, the NV center exhibits $C_{3v}$ symmetry, as illustrated in Fig. 1B. Electronic states are thus characterized by how they transform under $C_{3v}$ operations. $A_1$ energy levels consist of a single state which transforms into itself, with no sign change, under all symmetry operations. $A_2$ levels are also non-degenerate, but the state picks up a negative sign under reflections. Finally, $E$ levels consist of a pair of states, which transform into each other the way that the vectors $\hat{x}$ and $\hat{y}$ transform into each other under $C_{3v}$ symmetry operations. For more details on $C_{3v}$ symmetry and group theory, see Appendix of L. Childress' thesis. [3]

## Electronic structure

Although a number of efforts have been made to elucidate the electronic structure of the NV center from first principles, [4][5][6] it remains a topic of current research. Experimentally, it has been established that the NV center exists in two charge states, $NV^0$ and $NV^-$, with the neutral state exhibiting a zero-phonon line (ZPL) at 575nm and the singly charged state at 637nm (1.945 eV).[7] In this work we consider exclusively $NV^-$, which is dominant in natural diamond, and will refer to it simply as the NV center. The electron configuration for the neutron $NV^0$ center is a follows. The five valence electrons of the nitrogen atom form covalent bonds with the

three nearest neighbor carbon atoms while the remaining two form a lone pair that points in the direction of the neighboring carbon vacancy. The three unpaired valence electrons of the carbon atoms adjacent to the carbon vacancy occupy molecular orbitals. Two of these electrons occupy the lowest energy orbital with antiparallel spins while the third spin is unpaired. The $NV^0$ center is paramagnetic with spin S=1/2. The charged $NV^-$ center is formed by addition of one more electron which combines with the unpaired electron of $NV^0$ to form a spin S=1.

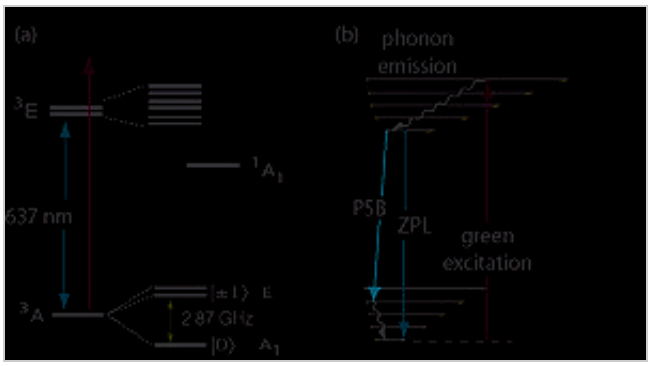


Figure 2. (a) The electronic structure of the NV center. The orbital states are indicated on the left hand side, and the spin-spin splitting of the ground state is indicated on the right hand side. After accounting for all spin-orbit, spin-spin, and strain perturbations, the structure of the six electronic excited states remains a topic of current research. Vibronic sideband transitions used in excitation are indicated by the yellow continuum. (b) The level diagram corresponding to ground and excited electronic states (manifolds), including the effect of lattice vibrations. The phonon relaxation within each of the manifolds is very fast, and the individual vibrational states can not be resolved. When the NV center is excited with green light (532 nm), it rapidly relaxes to the lowest vibrational state within the excited electronic manifold via phonon emission. The spontaneous photon decay of the electronic excited state (measured in our experiments) can occur directly into the ground state (Zero Phonon Line, ZPL, 637 nm) or into excited vibrational states (Phonon Side Band, PSB), from which it relaxes rapidly into the ground state via phonon emission.

The NV center has $C_{3v}$ symmetry, with the ZPL emission band associated with an *A* to *E* dipole transition. Hole-burning,[8] electron spin resonance (ESR), [9][10] optically detected magnetic resonance (ODMR),[11] and Raman heterodyne[12] experiments have established that the ground electronic state is a spin triplet $^3A_2$. This triplet is itself split by spin-spin interactions, yielding one state with $m_s = 0$ with $A_1$ character and two $m_s = \pm 1$ states with *E* character [13] which are 2.87 GHz higher in energy. Together with the 637nm ZPL, the 2.87 GHz zero-field ground-state splitting allows identification of a defect in diamond as an NV center.

In addition to the discrete electronic excited states which contribute to the ZPL, there are a continuum of vibronic excited states which appear at higher frequencies in absorption and lower frequencies in emission. When the vibronic states are excited using for example a 532 nm laser, phonon relaxation brings the NV center quickly into one of the electronic excited states. The NV center then fluoresces either via emission of 637 nm ZPL photon, or via a process in which photon emission is accompanied by a phonon (the so-called phonon sideband). The fluorescence in phonon sideband (PSB) is lower in frequency than that of ZPL, and extends from 650-800 nm. In practice, fluorescence into the ZPL accounts for only a few percent of the emitted light,[14] thus in the experiment broadband PSB fluorescence is collected.

# Experiment

Many of the early experiments on NV centers looked at ensemble properties, averaging over orientation, strain, and other inhomogeneities. Recently, confocal microscopy techniques have enabled examination of single NV centers, [15] permitting a variety of new experiments studying photon correlation statistics,[16][17] single optical transitions,[18] coupling to nearby spins,[19] and other effects difficult or impossible to observe in ensemble studies.

To study NV centers in diamond, we use a scanning confocal microscope incorporating magnetic field control and microwave coupling. The confocal microscope[20] uses point illumination and detection along the identical path, in order to increase the signal to noise ratio.The essential features of the apparatus are shown in Fig. 3.

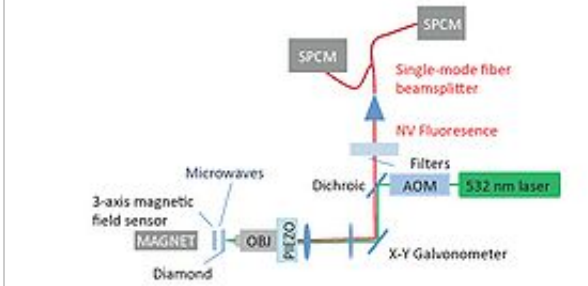


Figure 3. Diagram of the experimental setup.

The sample we use is a type IIa diamond specially selected for low nitrogen content ($\ll 1ppm$). This low nitrogen content is critical for observing coherent processes of the NV spin degree of freedom, because the electron spin associated with nitrogen donors interacts strongly with the NV center spin.[21] In the experiment, we study the NV centers that occur naturally in bulk diamond.

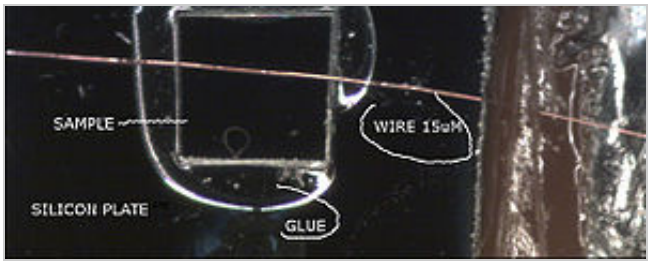


Figure 4. Diamond plate is mounted on a silicon wafer. It is subjected to a microwave field via a copper wire.

Our measurements rely on optically exciting a single NV within the sample, and detecting its fluorescence. Excitation into the vibronic sideband of the NV center is performed using a 532 nm doubled-YAG laser. The excitation beam passes through a fast Acousto-Optic Modulator (AOM) (rise time $\sim 2.5ns$), allowing pulsed excitation with widths of less than 100 ns, and are focused onto the sample with an oil immersion lens (Nikon Plan Fluor 100x NA 1.30).

To control the position of the focal spot on the sample we employ a closed-loop X-Y galvanometer combined with a piezo objective mount for focus adjustment. The mirrors forming the galvanometer are imaged onto the back of the objective, so that they vary the position of the focal spot without affecting the transmitted laser power. Scanning the galvanometer mirrors thus allows us to scan the focal spot over a plane in the sample, with a maximum scan range of about 100 x 100 $\mu m^2$.

Fluorescence from an NV center is collected by the same optical train, so that the detection spot is scanned along with the excitation spot. The fluorescence into the phonon sideband (650-800nm) passes through the dichroic mirrors (which combine the excitation lasers with the optical train), and a 600 nm long-pass filter before being coupled into a single-mode fiber. In many confocal setups, the point source emission is imaged onto a pinhole for background rejection; in our setup, the single-mode fiber replaces the pinhole. Ideally, this constitutes mode-matching between the mode collected by the objective from the NV center point source and the mode of the fiber. The fiber is itself acts as a beamsplitter, whose two outputs are connected to fiber-coupled single photon counting modules (SPCMs, Perkin-Elmer). Overall, the collection efficiency for fluorescence from the sample is just under $1\%$.

To apply strong microwaves to the NV center, the sample is mounted on a circuit board with a microwave stripline leading to and away from it. A 20 $\mu m$ copper wire placed over the sample is soldered to the striplines. By considering NV centers close to the wire, we can achieve large amplitudes for the oscillating magnetic field with modest microwave power through the wire.

A static applied magnetic field can be varied using a permanent magnet mounted on a three axis translational stage. To measure the magnetic field, a three-axis Hall sensor is mounted close to the sample. In addition, the NV center itself can be used as a magnetometer to measure the component of the magnetic field along the NV axis.

# Isolation of single NV centers: single photon source

The small excitation and detection volume of our confocal microscope, combined with the low concentration of NV centers in the sample, allows us to image single NV centers. Scanning the focal spot of the microscope over the sample reveals scattered bright spots of similar intensity. We can position the focus on top of one of the bright spots and examine its fluorescence. Several observations can be made to verify that the signal originates from the NV centers. First, the NV centers are photo-stable, i.e. fluorescence should not blink or disappear. Second, photon-count rate associated with single atom emission should undergo saturation as the intensity of the excitation laser is increased.

Assuming that the the excited state lifetime of NV centers is known or could be found from independent measurements (as discussed below), the saturation curve can be used for calibration of the excitation rate for a given laser intensity. Make a simple model to predict a fractional form of saturation. Using this model and saturation measurements, you can find the correspondence between the excitation rate and a laser power for any given NV center.

To verify that the observed signals are from single quantum emitters, photon correlation measurements can be used. One important quantum mechanical property of the radiation field is its statistics. The radiation from thermal sources (like a lamp) or coherent sources (like laser) is characterized by a distribution of photon numbers. A sequence of measurements on nominally identical weak pulses produced by such sources will reveal fluctuations in photon number associated with quantum nature of such pulses. In contrast, a single atom emitter is incapable of producing more than one photon at a time and can therefore serve as a source of single photons. In principle, one could observe this effect by histogramming the time interval between different photons, and examining the distribution close to zero delay. If the source was a single quantum emitter, the probability for a delay $\tau$ between successive photons should vanish as $\tau \to 0$. Owing to dead-time effects for avalanche photodetectors, such as the SPCMs we use, it is impossible to make such a measurement directly. To circumvent this problem it is necessary to divide the emitted photons between two detectors, and measure the time interval $\tau$ between a click in one detector and a click in the second detector. In the limit of low count rates, this measurement yields the probability of measuring a photon at time $\tau$ conditional on detection of a photon at time $0$, which corresponds to a two-time expectation value for the fluorescence intensity correlation function, $\langle I(\tau)I(0)\rangle$. Normalizing this quantity to the overall intensity $\langle I\rangle$ yields the second order correlation function for a stationary process

$$g^{(2)}(\tau) = \frac{\langle I(\tau)I(0)\rangle}{|\langle I\rangle|^2}.$$

Ideally, we should observe $g^{(2)}(0) = 0$ for emission from a single quantum emitter, whereas classical sources must have $g^{(2)}(0) \geq 1$.[22] Since a two-photon state has $g^{(2)} = 1/2$, observation of $g^{(2)}(0) < 1/2$ is sufficient to show that the photons are emitted one at a time by a single quantum system. The physical origin of vanishing coincidence probability for a perfect single photon source can be understood as follows. When a single photon arrives at a beamsplitter, it is either transmitted or reflected, resulting in a single photodetector click, and vanishing coincidence at $\tau = 0$. Such a behavior of photon-photon correlation function represents

direct evidence for quantum mechanical nature of light field. This is one of the most fundamental phenomena in quantum optics.[23]

Development of single photon sources is an active field of modern research. The NV center has received considerable attention as a robust, room temperature source of single photons, [24][25][26][27] and it is currently being used for quantum key distribution and other applications.

Photon correlation measurements and, specifically, the width of the anti-correlation feature can be used to quantify population dynamics of the NV center. Intuitively, the counter board measures the probability of photon emission (proportional to population of excited state, $n_e$, as a function of time, triggered by an initial photon emission that prepares the NV center in its ground state. Using the rate equation model one finds that $n_e = R/(R+\gamma)(1-\exp\left[-(R+\gamma)t\right])$ (show this!), where $R$ is optical excitation rate, proportional to light intensity and $\gamma$ is total decay rate from the excited state.[28][29] In your experiment, you can measure photon correlations for different pump powers and try to use the power dependence to determine the excited state lifetime.

# Spin properties of the NV center

While discussing the electronic structure of the NV center, we have already touched upon the existence of an $S = 1$ spin degree of freedom in the ground and excited states. In this section, we will consider in greater detail the interplay between optical transitions and the spin degree of freedom.

## Optically induced spin polarization

Early experiments established that the NV center spin shows a finite polarization under optical illumination with green light (see Fig. 2). Over the years, it has been determined that optical excitation causes the ground $m_s = 0$ state to become occupied with high probability, and recent measurements indicates that nearly full polarization may occur.[30] Nevertheless, the precise mechanism for optically induced spin polarization is still a topic of active research.[31][32]

Spin polarization originates due to existence of a singlet electronic state whose energy level lies between the ground and excited state triplets (see Fig. 2). Transitions into this singlet state occur primarily from $m_s = \pm 1$ states, whereas decay from the singlet leads primarily to the $m_s = 0$ ground state.[33] If the remaining optical transitions are spin-preserving, this mechanism should fully polarize the NV center into the $m_s = 0$ ground state.

## Spin-dependent fluorescence

Most current research on the NV center in diamond relies on optical detection of its ground state spin. Experimentally, an NV center prepared in the $m_s = 0$ state fluoresces more strongly than an NV center prepared in the $m_s = \pm 1$ state.[34] Optically detected magnetic resonance in the NV center was observed first at low temperature in ensemble studies.[35][36] At room temperature, this allows for efficient detection of the average spin population; using resonant excitation at low temperature, the effect is more pronounced, and single-shot readout is possible.

Specifically, at room temperature, the same mechanism which leads to optical spin polarization provides the means to optically detect the spin state. Non-resonant green excitation (at e.g. 532 nm) excites transitions from both the $m_s = 0$ and $m_s = \pm 1$ ground state levels. However, because the intersystem crossing occurs primarily from the $m_s = \pm 1$ excited state, population in $m_s = \pm 1$ ground state undergoes fewer fluorescence cycles before shelving in the singlet state for around 300 ns. The $m_s = \pm 1$ states thus fluoresce less than the $m_s = 0$ state, with a difference of $\sim 20 - 40\%$. [37][38][39]

# Single spin magnetic resonance: experiments

The electron spin of an NV center can be polarized and measured using optical excitation, as discussed above. By tuning an applied microwave field in resonance with its transitions, the spin can also be readily manipulated. Although it is difficult to address a single spin with microwaves, one can prepare and observe a single spin by confining the optical excitation volume to a single NV center. These ingredients provide a straightforward means to prepare, manipulate, and measure a single electronic spin in the solid state at room temperature.[40]

The experiments involving the NV electron spin can be roughly divided into continuous-wave (CW) and pulsed experiments. In both cases, we isolate a single spin using confocal microscopy and apply microwaves to it using a 20 μ*m* copper wire drawn over the surface of the sample (Fig. 4).

## Continuous-wave experiments

For continuous-wave (CW) measurements, microwave and optical excitation are applied at constant power to the NV center, and the fluorescence intensity into the phonon sideband is measured as a function of microwave frequency. The continuous 532 nm excitation polarizes the electron spin into the brighter $m_s = 0$ state; when the microwave frequency is resonant with one of the spin transitions $m_s = 0 \rightarrow m_s = \pm 1$, the population is redistributed between the two levels, and the fluorescence level decreases. In the absence of an applied magnetic field, the electron spin resonance (ESR) signal occurs at 2.87 GHz, while in a finite magnetic field the two transitions are shifted apart by $\sim m_s \cdot$ 2.8 MHz/Gauss.

In this experiment, you will observe and explore single spin ESR signal. Explore experimentally and explain how does this signal depend on applied microwave and optical power. Make a model for power dependance and check its consistency with excitation rate measurements. Explore how the signal changes with applied magnetic field.

Once the signal is optimized, close examination of a single $m_s = 0 \rightarrow m_s = \pm 1$ transition may reveal hyperfine structure associated with the nitrogen forming the NV center. Some NV centers have a structure that makes the hyperfine splitting more obvious. The $I = 1$ $^{14}N$ nuclear spin has a hyperfine structure which is governed by the Hamiltonian[41]

$$H^{(N)} = A_{\parallel}^{(N)} S_z I_z^{(N)} + A_{\perp}^{(N)} \left( S_x I_x^{(N)} + S_y I_y^{(N)} \right) + P \left( (I_z^{(N)})^2 - \frac{1}{3} (I^{(N)})^2 \right),$$

where $I^{(N)}$ is the nitrogen nuclear spin and $S$ is the NV center electron spin. A strong quadrupole interaction splits the $m_N = \pm 1$ states off from the $m_N = 0$ state by $P \approx 5$ MHz,[42] effectively freezing the orientation of the nitrogen nuclear spin for magnetic fields $\ll 1$ Tesla. In addition, the $^{14}N$ nuclear spin $I_N$

interacts with the electron spin $S$, so that in the electron spin excited state $m_s = 1$, the $m_N = \pm 1$ states are split from the $m_N = 0$ state by $P + A_{||}^{(N)}$ and $P - A_{||}^{(N)}$. Since the electron spin resonance transitions cannot change the nuclear spin state, the three allowed transitions are separated by $A_{||}^{(N)} \approx 2.2$ MHz. To resolve hyperfine structure, you will need to turn down the optical and microwave power such that the resulting linewidths are below $A_{||}^{(N)}$. For laser power of a few milliWatts, a factor of 100 attenuation is typical; microwave power has to be reduced in tandem.

These CW measurements served primarily as a means to calibrate the frequency of microwave excitation appropriate for pulsed experiments. However, the $^{14}$N hyperfine structure illustrates that CW measurements can also be useful for determining interaction strengths between the NV electron spin and other nearby spins.

## Pulsed microwave experiments

Continuous-wave spectroscopy provides a means to measure the energy levels of the NV spin system. To observe the spin dynamics, we must move to the time domain, and apply pulses of resonant microwaves. The excitation sequence for pulsed microwave experiments is illustrated in Fig. 5A. All experiments begin with electron spin polarization and end with electron spin measurement, both of which are accomplished using 532 nm excitation. In between, different microwave pulse sequences can be applied to manipulate the electron spin.

### Rabi oscillations

In a small applied magnetic field, the $m_s = 0$ to $m_s = 1$ spin transition of the NV center constitutes an effective two-level system. Driving this transition with resonant microwave excitation will thus induce population oscillations between the ground $m_s = 0$ and excited $m_s = 1$ states; these are known as Rabi oscillations.[43] To observe Rabi nutations, we drive the transition with a resonant microwave pulse of varying duration $t$ and measure the population remaining in $m_s = 0$. Fig.5B shows a typical Rabi signal.

For resonant microwave excitation, Rabi oscillations correspond to complete state transfer between $m_s = 0$ and $m_s = 1$. This allows us to calibrate our measurement tool in terms of the population $p$ in the $m_s = 0$ state. As shown in Fig. 5B, we can identify the minimum in fluorescence with $p = 0$ and the maximum with $p = 1$. For weak or off-resonant microwave fields one employs a more careful analysis, which fits the data to a multi-level model including all of the hyperfine structure associated with the $^{14}$N nuclear spin and any other nearby spins. In either case, we can present data from more complicated pulsed experiments in units of $m_s = 0$ population $p$ obtained from fits to Rabi nutations observed under the same conditions.

The frequency $\Omega$ of the Rabi nutations depends on the microwave power $I_{MW}$ as $\Omega \propto \sqrt{I_{MW}}$. For a given microwave power, we observe Rabi nutations to calibrate the pulse length required to flip the spin from $m_s = 0$ to $m_s = 1$; this is known as a $\pi$ pulse, because it corresponds to half of the Rabi period. Shorter and longer pulses create superpositions of the spin eigenstates; in particular, a microwave $\theta$ pulse (i.e. of duration $\tau = \theta / \Omega$) sends the $m_s = 0$ state $|0\rangle$ into the superposition

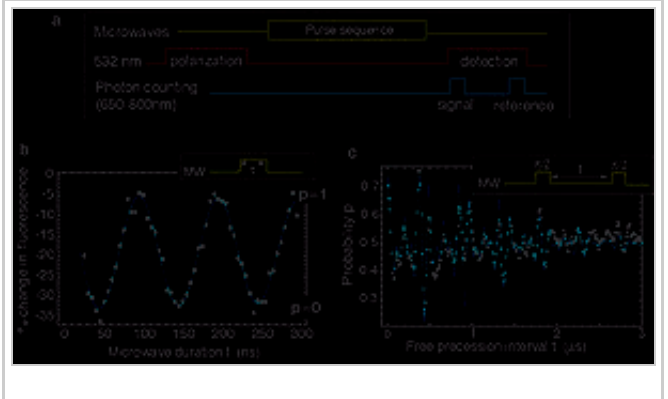

$\cos\theta|0\rangle + i\sin\theta|1\rangle$. This corresponds to rotating the effective spin-1/2 system $\{|0\rangle, |1\rangle\}$ by $\theta$ about an axis in the $\hat{x} - \hat{y}$ plane. The relative phase of the two components (or, equivalently, the orientation of the axis in the $\hat{x} - \hat{y}$ plane) is set by the phase of the microwave excitation. For a single pulse, this phase does not matter (it could equally well be incorporated into a redefinition of $|1\rangle$), but composite pulse sequences often make use of shifts in the microwave phase. As an example, a pulse A of duration $\theta_A$ followed by a $90$ degree phase shifted pulse B of duration $\theta_B$ would correspond to rotating the spin by $\theta_A$ around the $\hat{x}$ axis followed by a rotation by $\theta_B$ around the $\hat{y}$ axis.

Figure 5. Pulsed electron spin resonance. Pulse sequence for Rabi oscillation (a) and Ramsey sequence (b) experiments

**Ramsey fringes and spin echo**

Rabi nutations correspond to driven spin dynamics. We can also observe the free (undriven) spin dynamics by generating a superposition of the spin eigenstates $m_s = 0$ and $m_s = 1$, letting it evolve freely, and then converting the phase between the two eigenstates into a measurable population difference. This is accomplished using a Ramsey technique,[44] which consists of the microwave pulse sequence $\pi/2 - \tau - \pi/2$ as illustrated in the inset to Fig. 5C. For a simple two-level system, the Ramsey sequence leads to population oscillations with a frequency equal to the microwave detuning $\delta$. Because of the $^{14}$N hyperfine structure, we observe a more complex signal from three independent two-level systems. These three signals beat together, producing the complicated pattern shown in Fig. 5C. The data can be modeled with three superposed cosines, corresponding to the three hyperfine transitions.

The fit to the Ramsey data should also include an overall envelope such as Gaussian envelope $e^{(-\tau/T_2^*)^2}$, which decays on a timescale $T_2^*$ known as the electron spin dephasing time. The dephasing time is the timescale on which the two spin states $m_s = 0$ and $m_s = 1$ accumulate random phase shifts relative to one another. For the NV center, these random phase shifts arise primarily from the effective magnetic field created by a complicated but slowly-varying nuclear spin environment. These frequency shifts can be eliminated by using a spin-echo (or Hahn echo) technique.[45] It can be used to extend the coherence time and to gain addition insights into spin dynamics.

Spin echo consists of the sequence $\pi/2 - \tau - \pi - \tau' - \pi/2$ (see Fig. 5A), where $\pi$ represents a microwave pulse of sufficient duration to flip the electron spin from $m_s = 0$ to $m_s = 1$, and $\tau$, $\tau'$ are durations of free precession intervals. As with the Ramsey sequence, the Hahn sequence begins by preparing a superposition of electron spin states $1/\sqrt{2}\,(|0\rangle + i|1\rangle)$ using a $\pi/2$ microwave pulse. This superposition precesses freely for a time $\tau$, so that, for example, the $|1\rangle$ component picks up a phase shift δτ relative to the $|0\rangle$ component, yielding $1/\sqrt{2}\left(|0\rangle + ie^{i\delta\tau}|1\rangle\right)$. The π pulse in the middle of the spin-echo sequence flips the spin, resulting in the state $1/\sqrt{2}\left(i|1\rangle - ie^{i\delta\tau}|0\rangle\right)$. Assuming that the environment has not changed since the first free precession interval, the $|1\rangle$ component will pick up the phase $\delta\tau'$ during the second free precession interval, leaving the system in the state $1/\sqrt{2}\left(ie^{i\delta\tau'}|1\rangle - ie^{i\delta\tau}|0\rangle\right)$. When the two wait times are precisely equal, $\tau = \tau'$, the random phase shift factors out, so the final $\pi/2$ pulse puts all of the population back into $|0\rangle$. When the wait times are unequal, the Hahn sequence behaves like a Ramsey sequence with a delay $\tau - \tau'$.

Spin echo is widely used in bulk electron spin resonance (ESR) experiments to study interactions and determine the structure of complex molecules.[46] Likewise, spin-echo spectroscopy provides a useful tool for understanding the complex mesoscopic environment of a single NV center: by observing the spin-echo signal peak ($\tau = \tau'$), we can decouple spin dynamics from low-frequency environment, extend its coherent evolution and can indirectly glean details about the environment itself.

Finally, spin echo and other related decoupling techniques constitute an important tool for extending coherence times of spin qubits. Applications of such techniques ranging from quantum computation to nanoscale magnetometry are at the forefront of the modern research.

# Photos

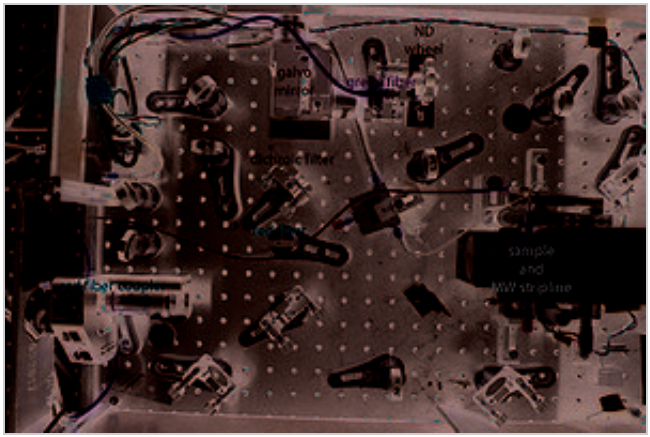

Confocal microscope.

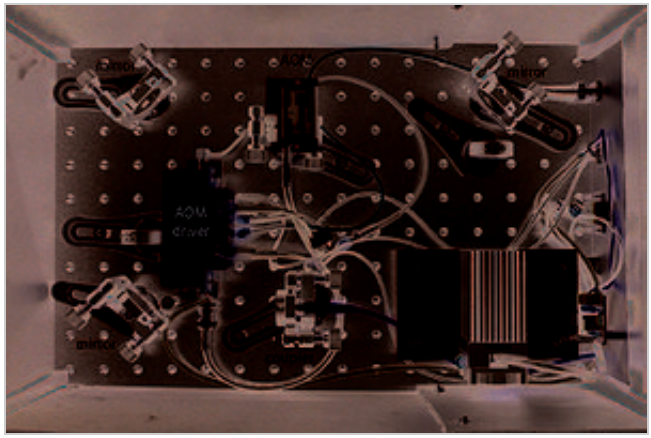

Laser.

# Apparatus

## Confocal Microscope

A confocal microscope illuminates a small region of a sample with a focussed laser beam and fluorescence is detected from the same region. The beam scans across the sample by means of a 2D rotating mirror galvanometer. A schematic diagram of the optics is given below. Three separate enclosed optical breadboards house a laser, detectors, and the confocal microscope respectively. See the photos below. These breadboards are in turn mounted on a Thorlabs PTR11104 optical table.

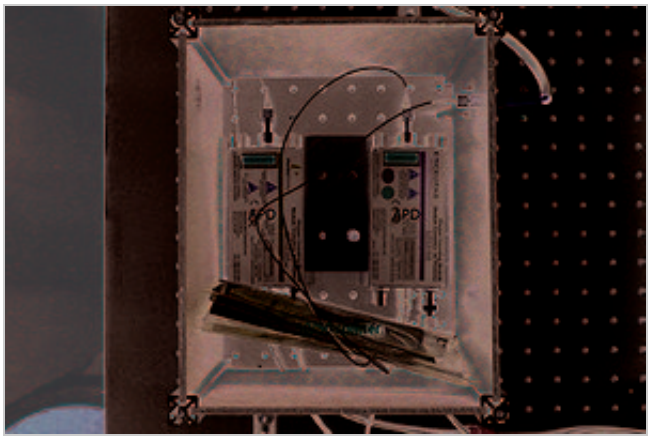

Detectors.

Accurate optical alignment is critical. Consult the faculty or staff before changing the position or angle of any optics.

### Laser

The light source is a frequency-doubled diode-pumped Nd-YAG laser. An infrared laser diode pumps a crystal of yttrium aluminum garnet doped with neodymium. The neodymium ions emit light at 1064 nm which is

frequency-doubled in a crystal of potassium dihydrogen phosphate (KDP). The nominal power of the laser is 200 mW. If you open the laser box when the laser is on, use the Thorlabs LG-10 laser safety glasses to block both the 532 nm and 1064 nm light.

The laser power supply is housed in a small black box with a key switch. As a safety precaution return the key to the blue cabinet at the end of each lab session.

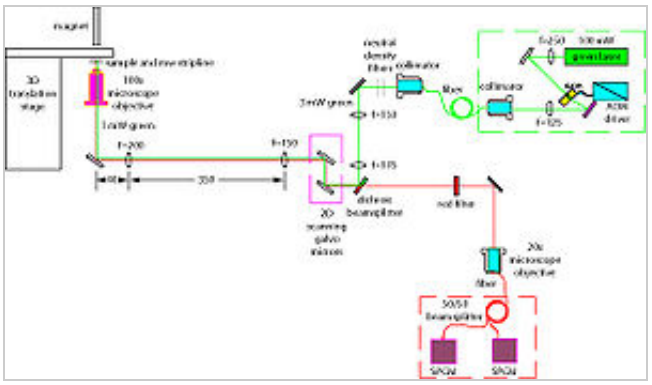

Confocal microscope block diagram.

**Acousto-optic modulator: Crystal Technology 3080-125/controller 1080AF-DIFO-1.0**

An acousto-optic modulator mounted in the laser box switches the light output off and on. The optical element of an AOM is a crystal of tellurium dioxide. A piezo-electric transducer mounted on the crystal produces an acoustic wave in the crystal in response to an rf voltage across it. The light diffracts from the acoustic wave in a process similar to Bragg reflection. Two output beams are generated: a zero-order beam which is simply transmitted through the TeO$_2$, and a diffracted beam which is coupled to a fiber.

**Green fiber**

A single mode fiber, Thorlabs P1-630A-FC-2, transmits light from the laser box to the confocal microscope box. As currently configured (Spring 2012) the output of the fiber is approximately 3 mW. The "mode field diameter" of the fiber is 4.3 microns. The fiber does not transmit 1064 nm light efficiently.

A Thorlabs F230FC-B fiber collimator couples the free space laser beam into the fiber in the green laser box. A Thorlabs CFC-8X-A adjustable collimator is used at the other end of the fiber in the confocal microscope box. The focal length of this collimator is 7.5 mm and the output beam waist diameter is 1.2 mm.

**Neutral density filters**

Immediately downstream of the fiber coupler is a filter wheel housing neutral density filters. Use these to attenuate the laser power. Nominal values of the filters are given in the table. For additional attenuation use the ND 1.0 filter mounted on a one-inch post.

| number on filter wheel | attenuation (log scale) | transmission (linear scale) |
|---|---|---|
| 1 | 0.0 | 1.00 |
| 2 | 0.1 | 0.79 |
| 3 | 0.2 | 0.63 |
| 4 | 0.3 | 0.50 |
| 5 | 0.5 | 0.32 |
| 6 | 1.0 | 0.10 |

**Home Made Power Meter**

A photodiode mounted on a moveable post is used to measure the laser power leaving the fiber. To measure the

laser power, place the photodiode downstream of the ND filters and switch the multimeter to dc current $\mu Amps$. The calibration is: 2.76 mW / 275 microAmps. This is a typical power used to excite the NVs in the diamond sample. %If you find less than 2 mW, cycle power to the laser.

**Galvo-controlled mirrors: Thorlabs GVS012**

In order to locate NV centers in the diamond plate, there is an xyz translation stage for course movement, and galvo controlled mirrors for fine movement. The mirrors, mounted on motor-controlled shafts are used to make small changes in the angle of the laser beam. These are dc motors which receive power under control of the LabVIEW software at the rate of 1.25 degree/Volt. The *Galvo Controls* tab has buttons for increasing and decreasing the galvo voltages. The Arrow keys on the computer keyboard are shortcuts for up/down and right/left.

**Scanning microscope: principle of operation**

As the galvo mirrors change the angle of the beam during a scan, we require that the green and red beams remain colinear. If this were not the case, detection would be impossible since the red beam would miss the fiber for some range of the galvo mirrors' travel. To meet this requirement, an optical trick is employed. The lens in the figure refers to a composite of three actual lenses: the pair of lenses downstream of the mirrors plus the objective. The galvo mirrors and the sample plane are placed into the front and back focal planes of the composite lens, respectively. In this case, the collimated portions of the beams remain colinear.

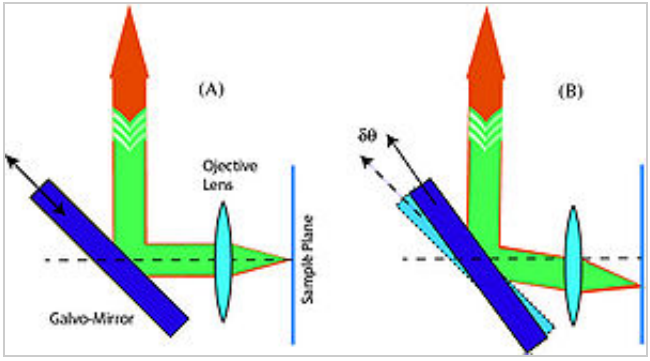

Principle of confocal microscope. The Galvo mirror and the sample plane are placed into the front and back focal planes of the lens, respectively. In such a case, the excitation path (green) and collection path (red) can be identical.

This telescope as well as one upstream of the galvo mirrors are chosen so that the beam diameter matches the size of the objective's rear aperture to make the sharpest possible focus.

**Objective: Nikon MRH01902 CFI Plan Fluor 100x Oil Immersion**

The Nikon objective has magnification 100x and working distance of 0.2 mm. The numerical aperture is 1.30 and the effective focal length is 2 mm. The field of view is 0.18 mm. The immersion oil has high viscosity and normally does not need to be refreshed between experimental runs.

**Sample**

The sample is a type IIa (high purity) diamond selected for low nitrogen content. It is a natural diamond originating in the Ural Mountains. The sample is epoxied to a silicon substrate. Silicon is chosen because it absorbs approximately 70\% of the incident green light, and does not emit red fluorescence.

Under normal operation, it is not advisable to remove the sample for viewing. A photo is included in the "Experiment" section above.

**Translation stage: Newport 562-XYZ**

The sample is mounted on a stainless steel translation stage. The translation stage is used for coarse positioning during alignment. Under normal operation, it is not advisable to move the translation stage.

However fine control of focussing is accomplished with a piezoelectric transducer mounted under the vertical micrometer screw. Voltage is applied to the PZT by a Thorlabs MDT693A piezo controller which in turn receives an input control signal from the NI 6323 under control of LabVIEW. The \emph{Galvo Controls} tab has buttons for increasing and decreasing the PZT voltage. The Page Up/Page Down keys are shortcuts for the Shallower/Deeper.

**Dichroic beamsplitter: Semrock LM01-552-25**

The dichroic beamsplitter reflects green and transmits red. The beamsplitter separates the red detection beam from the green excitation beam.

**Red detection**

In order to reject green light scattered from the sample, a long pass filter, Omega Optical 3RD600LP is placed downstream of the dichroic beamsplitter. The transmission of the dichroic beamsplitter is one percent at 532 nm whereas the transmission of the long-pass filter is only 10$^{-6}$ whereas the red transmission is greater than 80\%. The red light is focused by a second microscope objective, an Olympus 20X objective with NA 0.4. The working distance is 1.2 mm and the focal length is 9 mm. A New Focus 9091 fiber coupler has fine controls for the position and angle of a fiber. The fiber connector (Summer 2012) is slightly flaky. You may find the fiber tied down with cable ties for this reason. This fiber leads to a Thorlabs FC632-50B-FC 50/50 beam splitter which delivers red photons to the two detectors.

**Single Photon Counting Modules: Perkin Elmer SPCM-AQR-14-FC**

A pair of avalanche photodiodes (APDs) detect red light emitted by NVs in the diamond sample. An APD is similar to an ordinary photodiode in that an incident photon strikes the depletion region of a p-n junction, creating an electron-hole pair. The APD is different from a photodiode in the sense that a large reverse bias across the depletion region creates an avalanche effect. A single electron liberates many secondary electrons, each of which liberate many more secondary electrons and so on. Thus a single photon can generate a large electrical signal. This is the same process that takes place in photomultiplier tubes, but all within a compact solid state device. The dark count for the SPCM-AQR-14 is less than 100 counts/sec. Dead time after an event is 50 ns. The APD output is a TTL pulse of 2.5 Volts minimum. The quantum efficiency is greater than 50% at 650 nm and greater than 35% at 830 nm.

## National Instruments PCIe-6323 X Series Multifunction ePCI card

The National Instruments 6323 Data Acquisition card interfaces the computer with the confocal microscope. Four analog outputs control both galvo motors, the PZT and the microwave attenuator. Counter/timers count pulses from the APDs, synchronize counting with the microwave sweep and count pulses from the SpinCore pulse generator card.

A rack-mounted breakout box, National Instruments BNC-2090A incorporates a rear-panel connector matching the connectors on the 6323 to front-panel BNC connectors.

## LabVIEW program NV_191.vi

(courtesy of Mike Goldman)

A LabVIEW program written by the Lukin group controls the experiment and acquires data. Referring to the figure, zones A through G are a collection of controls and indicators. Data files can be saved using the controls in the lower right.

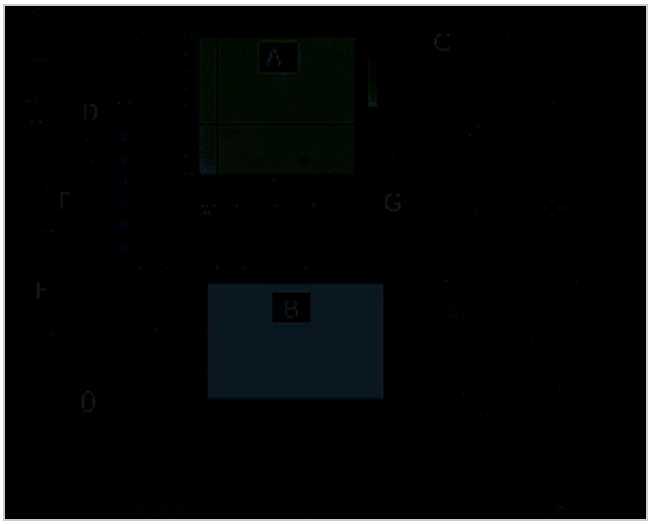

Front panel of NV LabVIEW program.

- **Zone A** is a map showing the intensity of red light emitted by the sample. Scanning an appropriate area is important since you may not see NVs if the resolution is too low. Typical scan range is 0.2 V in X and Y which corresponds to about 8 microns. As of summer 2012, bright NVs can be seen in the range X = [-0.1 V, +0.1 V], Y = [-0.4 V, -0.2 V]. This is for micrometer settings X = 6.318 mm, Y = 7.555 mm and Z = 6.023 mm. You can look anywhere in the sample for NVs. To expedite your experiment, consider using established parameters.
- **Zone B** is a data window which varies from tab to tab. The "Counter Readout" tab is shown.
- **Zone C** selects the active set of controls. The box below Zone C shows controls for Galvo Positioning', PicoHarp, Microwave, Pulse Experiment, etc.
- The box above **Zone D** contains controls for the Galvo Scan. The buttons below are start and stop controls for Galvo Scan, Counter, NV lock, Microwave scan, Picoharp, and Pulse Experiments.
- **Zone E** is the Optimize button -- important enough to have its own zone. The stability of the NV count rate is usually good enough to make measurements for several minutes, but there is a tendency to drift. Small changes in position caused by temperature fluctuation and other factors cause the signal to change over time. "Optimize" is a routine which scans a small range of X and Y, looking for maximum signal. Optimize before starting each data run. "NV lock" is automatic "Optimizing."
- **Zone F** is a set of tabs:
  - *Counter Readout* is a graph of total counts (sum of two APDs) as a function of time.
  - *NV Tracking Fits* shows the fits computed by the "Optimize" routine.
  - *NV Tracking History gives several ways of monitoring the position of an NV.*
  - *MW Scan Result* is a graph of count rate synchronized with microwave sweep. Many sweeps are averaged and the result displayed.
  - *MW Scan History* is a color representation of every microwave sweep in the series of averages.
  - *Pulse Experiment* controls pulsed ESR experiments.
  - *PicoHarp* displays the result of g2 correlation measurements.

- **Zone G** activates the acousto-optic modulator, coupling the green laser light into the fiber, which in turn illuminates the confocal microscope.

## PicoQuant TimeHarp 200 PCI board for Time-Correlated Single Photon Counting

As discussed above in section 4, we wish to use the TimeHarp 200 to measure the second-order correlation function,

$$g^{(2)}(\tau) = \frac{\langle I(\tau)I(0)\rangle}{|\langle I\rangle|^2}$$

for the photons emitted by an NV center.

The TimeHarp card measures and digitizes the time interval between two photon events. Two APDs each receive approximately 50% of the NV photons and provide input pulses for the TimeHarp inputs SYNC and START. The SYNC input requires a fast negative pulse to trigger a measurement. A positive pulse in the range of 50 - 1500 mV at the START input stops the measurement. After a measurement, the time interval is added to a histogram of up to 4096 bins. The TimeHarp card has an incredibly small time resolution of 40 ps. However the dead time associated with each event is 350 ns.

Given the limitation of dead time, it is only possible to measure $g^{(2)}(\tau)$ when the count rate is low compared to the histogram bin duration. (Is this approximation valid for typical experimental parameters?) Suppose that the probability of detecting a photon in any particular time bin after a SYNC pulse is small. In this case most bins will have zero counts and one particular bin, $\tau'$ will receive one count and stop the measurement. The SYNC pulse corresponds to $I(0) = 1$ and $I(\tau) = 0$ for most time intervals. $I(\tau') = 1$. Thus $g^{(2)}(\tau') = 1$ apart from the normalizing factor $|\langle I\rangle|^2$. Repeating the measurement many times is necessary to build up a histogram with adequate statistics. The maximum number of TimeHarp histogram bins is 4096.

We wish to observe $g^{(2)} < 1$ on a time scale smaller than the dead time of both the APDs and the TimeHarp. To circumvent the APD dead time, we split the signal into two APDs. To circumvent the TimeHarp dead time, a length of coaxial cable is inserted into the SYNC channel, moving the feature of interest to a time much longer than the dead time. Since the APDs are nominally identical, in principle the delay could be in either channel.

The LabVIEW **Controls to View: Picoharp Settings** tab contains six controls. Typical parameters are mentioned in square brackets.

- **Resolution** [64 ps] is the bin size that the TimeHarp card uses to acquire data.
- **Acquisition time** [1000 ms] is the total time available for a single acquisition. The actual time required for a single measurement is determined by the resolution and the number of bins. Many measurements can be added to improve signal to noise ratio.
- **Channel 0 level** [100 mV]
- **Channel 1 level** [50 mV]
- **Channel 0 zero X** [5 mV]
- **Channel 1 zero X** [5 mV]

The **Counter Model** control must be set to **TimeHarp** for proper functioning of the TimeHarp card. However the word **PicoHarp** is used in the Zone F tab name interchangeably with **TimeHarp**. For technical reasons, the **Resolution** indicator in Zone F reads differently than the Zone C control. Saving data from the TimeHarp card is done automatically if the **Save Data** switch is turned on. Data can not be saved after a run completes.

## Microwave Source and Amplifier

The microwave source is controlled by LabVIEW through a USB interface, "COM3" as well as by analog output AO1-A. The analog voltage activates two MiniCircuits RVA33 attenuators. The attenuator control in the LabVIEW program give the output of the microwave synthesizer in dBm. The amplifier gain is + 45 dBm. The maximum amplifier output is 13 Watts.

The instrument bandwidth is from 2800 to 3000 MHz.

There are four analog inputs and three green indicator LEDs on the front panel of the microwave synthesizer:

**INPUTS**

- *OSC EXT* accepts an external clock signal. It is not normally used.
- *GATE* is used during pulse experiments such as Rabi oscillation. Input is accepted from PB0 of the SpinCore ESR-PRO-400.
- *SWEEP* is a pulse input from the NI6323 User1-B which starts a microwave sweep.
- *ATTEN* requires analog voltages from zero to 5 Volts from the NI6323 analog output AO1-A

**INDICATORS**

- *Output active* lights when the microwave source is providing output.
- *Initialize* is on briefly when LabVIEW initializes communication.
- *Oscillator Locked* should light at all times when the unit is in use. This indicates that the microwave frequency is stable.

A schematic diagram of the microwave source is available in the bench notes.

An antenna and microwave detector, Telonic XD-23E can also be used to measure radiated microwave power in arbitrary units.

## Electronics block diagram

For reference, a diagram showing all electrical connections is included in the bench notes. An AutoCAD drawing with full resolution is available on the NV lab computer.

## SpinCore Technologies PulseBlaster ESR-PRO-400 PCI Pulse Generator Board

The pulse generator PCI card generates TTL pulses used in three separate applications. Output number 0 is a trigger pulse for the microwave generator. Output number 1 triggers the acousto-optic modulator. Output number 3 triggers microwave pulses for the Rabi and Ramsey experiments.

The minimum pulse duration is 2.5 ns. All outputs have 50 ohm impedance.

## Pulse Experiments

After completing the Continuous Wave ESR experiment with external magnetic field, one is in a position to carry out experiments with pulsed microwaves. Select one of the resonances and fix the microwave frequency to match it. Turn OFF the microwaves. Set appropriate parameters in the Pulse Experiment control window (pictured at right). Details of the pulse sequences are given below.

All pulse experiments have to be repeated a large number of times to accumulate adequate statistics.

---

## Rabi

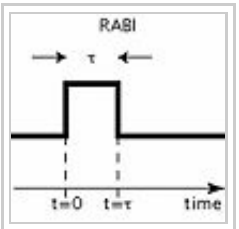

Microwave pulse sequence for Rabi oscillation.

Rabi oscillations correspond to varying probability for the NV center to be found in the $m_s = 0$ or $m_s = \pm 1$ spin states. A single resonant microwave pulse of variable duration is applied, and a pulse of green light "reads out" the NV center spin state.

The scan parameters *Minimum*, *Maximum* and *Step* set the range and increment of the microwave pulse duration. $\pi$ and $\pi/2$ times are not used.

A typical value for "Maximum" is 5000 ns when the microwave power is -21 dB. One can measure the Rabi period as a function of microwave power.

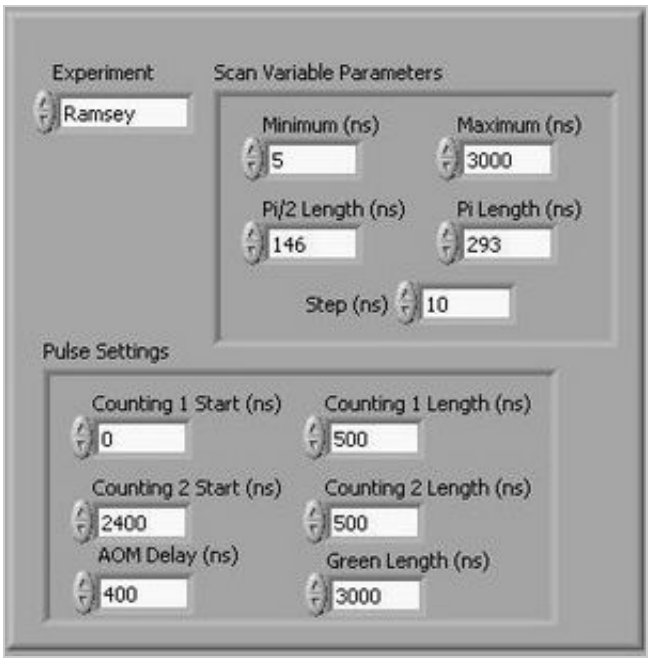

LabVIEW control panel for pulse settings.

---

## Ramsey

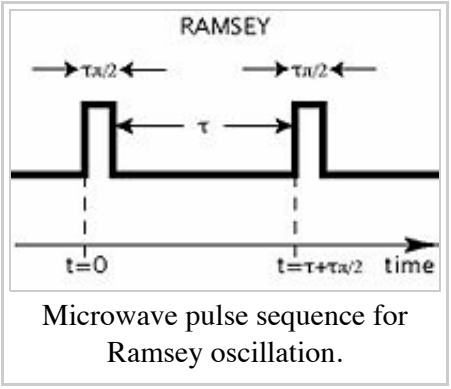

Microwave pulse sequence for Ramsey oscillation.

The Ramsey pulse sequence is a pair of $\pi/2$ pulses separated by a variable delay. *Minimum*, *Maximum* and *Step* set the range and increment of the delay. See the figure at left. The $\pi/2$ pulse should be set to one quarter of the Rabi period. $\pi$ time is not used.

---

## Hahn Echo

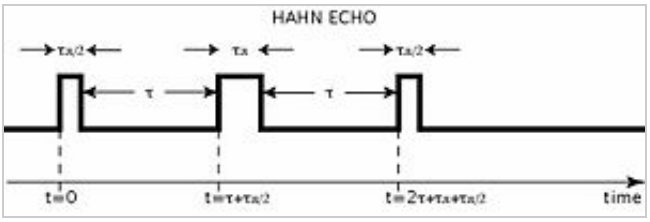

Microwave pulse sequence for Hahn echo.

The Hahn echo pulse sequence is a $\pi/2$ pulse followed by a $\pi$ pulse, followed by another $\pi/2$ pulse. The delay between pulses is the same, and *Minimum*, *Maximum* and *Step* set the range and increment of this delay. See the figure at left. The $\pi$ and $\pi/2$ pulses should be set to one quarter and one half the Rabi period respectively.

---

## Readout

In order to measure the probability of finding the NV center in the $m_s = 0$ state, a pulse of green light is used.

Refer to the figure at right. $T_{ReadOut}$ is the nominal start time, $t = 0$, for readout. $T_{ReadOut} = Maximum(ns) + 1000ns$ for Rabi and Ramsey pulse sequences. $T_{ReadOut} = 2 * Maximum(ns) + 1000ns$ for the Hahn Echo pulse sequence.

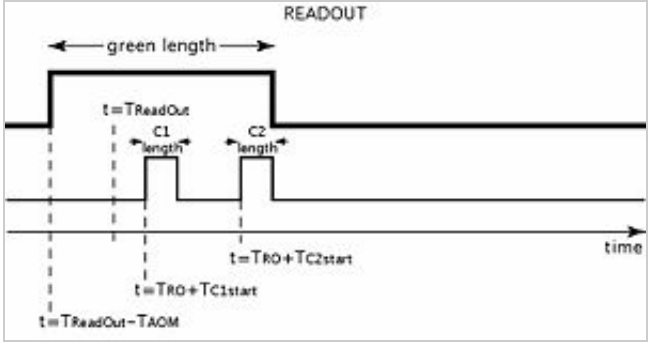

Green laser pulse and counter sequences for readout.

The green light actually comes on earlier by an amount $T_{AOM}$ since the Acousto-Optic Modulator has a finite rise time, unlike the square pulse shown.

The first counter window, defined by parameters *Counting*1*Start* and *Counting*1*Length*, gives the "signal count." The second counter window, defined by parameters *Counting*2*Start* and *Counting*2*Length*, gives the "reference count." The reference count can be used to normalize the signal count, compensating for drifts in alignment, green power, or other factors that influence the NV fluorescence rate.

There is no separate initialization green pulse. The readout poulse serves to reionize the NV center (with ~ 70% efficiency) and pump it into $m_s = 0$.

Typical parameters for readout are given in the table.

| | |
|---|---|
| Counting 1 Start | 0 ns |
| Counting 1 Length | 500 ns |
| Counting 2 Start | 2400 ns |
| Counting 2 Length | 500 ns |
| AOM Delay | 400 ns |
| Green Length | 3000ns |

HARDWARE CHANNELS

| | |
|---|---|
| BNC0 | MW gate |
| BNC1 | green |
| BNC2 | |
| BNC3 | counter gate |

# References


1. ↑ D. Bouwmeester, A. K. Ekert, and A. Zeilinger (Eds.). The physics of quantum information: quantum cryptography, quantum teleportation, quantum computation. Springer-Verlag, NY, 2000.
2. ↑ J. R. Maze, P. L. Stanwix, J. S. Hodges, S. Hong, J. M. Taylor, P. Cappellaro, L. Jiang, M. V. Gurudev Dutt, E. Togan, A. S. Zibrov, A. Yacoby, R. L. Walsworth, and M. D. Lukin. "Nanoscale magnetic sensing with an individual electronic spin in diamond (http://www.fas.harvard.edu/~phys191r/References/d4/Maze2008.pdf) ," Nature, 455:644–U41, October 2008.
3. ↑ Lilian Childress, "Coherent manipulation of single quantum systems in the solid state (http://www.fas.harvard.edu/~phys191r/References/d4/LilyThesis.pdf) ," Harvard University (2007).

4. ↑ A. Lenef and S.C. Rand. "Electronic structure of the n-v center in diamond: Theory (http://www.fas.harvard.edu/~phys191r/References/d4/Lenef1996b.pdf) ," Phys. Rev. B, 53:13441, 1996. and A. Lenef et. al. "Electronic structure of the n-v center in diamond: Experiment (http://www.fas.harvard.edu/~phys191r/References/d4/Lenef1996a.pdf) ," Phys. Rev. B, 53:13427, 1996.
5. ↑ J.P.D Martin. Fine structure of excited e-3 state in nitrogen-vacancy centre of diamond. J. Lumin., 81:237, 1999.
6. ↑ N.B. Manson, J.P. Harrison, and M.J. Sellars. "The nitrogen-vacancy center in diamond re-visited (http://www.fas.harvard.edu/~phys191r/References/d4/Manson2006.pdf) ," arXiv:cond-mat/0601360v2, 2006.
7. ↑ T. Gaebel et al. "Photochromism in single nitrogen-vacancy defect in diamond (http://www.fas.harvard.edu/~phys191r/References/d4/Gaebel2006b.pdf) ," Appl. Phys. B-Lasers and Optics, 82:243, 2006.
8. ↑ N.R.S Reddy, N.B. Manson, and E.R. Krausz. 2-laser spectral hole burning in a color center in diamond. J. Lumin., 38:46, 1987.
9. ↑ D.A Redman, S. Brown, R.H. Sands, and S.C. Rand. "Spin dynamics and electronic states of nv centers in diamond by epr and four-wave-mixing spectroscopy (http://www.fas.harvard.edu/~phys191r/References/d4/Redman1991.pdf) ," Phys. Rev. Lett., 67:3420, 1991.
10. ↑ J.H.H Loubser and J.A. van Wyk. "Electron spin resonance in the study of diamond (http://www.fas.harvard.edu/~phys191r/References/d4/Loubser1978.pdf) ," Rep. Prog. Phys., 41:1201, 1978.
11. ↑ E. van Oort, N.B. Manson, and M. Glasbeek. "Optically detected spin coherence of the diamond n-v centre in its triplet ground state (http://www.fas.harvard.edu/~phys191r/References/d4/vanOort1988.pdf) ," J. Phys. C: Solid State Phys., 21:4385, 1988.
12. ↑ N.B. Manson, X.-F. He, and P.T.H. Fisk. "Raman heterodyne detected electron-nuclear-double-resonance measurements of the nitrogen-vacancy center in diamond (http://www.fas.harvard.edu/~phys191r/References/d4/Manson1990.pdf) ," Opt. Lett., 15:1094, 1990.
13. ↑ N.B. Manson, J.P. Harrison, and M.J. Sellars. "The nitrogen-vacancy center in diamond re-visited (http://www.fas.harvard.edu/~phys191r/References/d4/Manson2006.pdf) ," arXiv:cond-mat/0601360v2, 2006.
14. ↑ F. Jelezko et al. "Spectroscopy of single n-v centers in diamond (http://www.fas.harvard.edu/~phys191r/References/d4/Jelezko2001.pdf) ," Single Mol., 2:255, 2001.
15. ↑ A. Gruber et al. "Scanning confocal optical microscopy and magnetic resonance on single defect centers (http://www.fas.harvard.edu/~phys191r/References/d4/Gruber1997.pdf) ," Science, 276:2012, 1997.
16. ↑ C. Kurtsiefer, S. Mayer, P. Zarda, and H. Weinfurter. "Stable solid-state source of single photons (http://www.fas.harvard.edu/~phys191r/References/d4/Kurtsiefer2000.pdf) ," Phys. Rev. Lett., 85:290, 2000
17. ↑ A. Beveratos et al. "Nonclassical radiation from diamond nanocrystals (http://www.fas.harvard.edu/~phys191r/References/d4/Beveratos2001.pdf) ." Phys. Rev. A, 64:061802(R), 2001.
18. ↑ Ph. Tamarat et al. "Stark shift control of single optical centers in diamond (http://www.fas.harvard.edu/~phys191r/References/d4/Tamarat2006.pdf) ," Phys. Rev. Lett., 97:083002, 2006.
19. ↑ F. Jelezko et al. "Observation of coherent oscillation of a single nuclear spin and realization of a two-qubit conditional quantum gate (http://www.fas.harvard.edu/~phys191r/References/d4/Jelezko2004.pdf) ," Phys. Rev. Lett., 93:130501, 2004.
20. ↑ Wikipedia. Confocal microscopy (http://en.wikipedia.org/wiki/Confocal_microscopy) .
21. ↑ R. J. Epstein, F. Mendoza, Y. K. Kato, and D. D. Awschalom. "Anisotropic interactions of a single spin

and dark-spin spectroscopy in diamond (http://www.fas.harvard.edu/~phys191r/References/d4/Epstein2005.pdf) ," Nature Physics, 1:94, 2005.
22. ↑ Leonard Mandel and Emil Wolf. Optical Coherence and Quantum Optics. Cambridge University Press, Berlin, 1995.
23. ↑ Roy J. Glauber. Nobel lecture: One hundred years of light quanta (http://www.nobelprize.org/nobel_prizes/physics/laureates/2005/glauber-lecture.html) .
24. ↑ C. Kurtsiefer, S. Mayer, P. Zarda, and H. Weinfurter. "Stable solid-state source of single photons (http://www.fas.harvard.edu/~phys191r/References/d4/Kurtsiefer2000.pdf) ," Phys. Rev. Lett., 85:290, 2000.
25. ↑ A. Beveratos et al. "Nonclassical radiation from diamond nanocrystals (http://www.fas.harvard.edu/~phys191r/References/d4/Beveratos2001.pdf) ." Phys. Rev. A, 64:061802(R), 2001.
26. ↑ A. Beveratos et al. "Single photon quantum cryptography (http://www.fas.harvard.edu/~phys191r/References/d4/Beveratos2002.pdf) ," Phys. Rev. Lett., 89:187901, 2002.
27. ↑ R. Alleaume, F. Treussart, G. Messin, Y. Demeige, J.F. Roch and A. Beveratos, R. Brouri, J.P. Poizat, and P. Grangier. "Experimental open air quantum key distribution with a single photon source (http://www.fas.harvard.edu/~phys191r/References/d4/Alleaume2004.pdf) ," arXiv:quant-ph/0402110v1, 2004.
28. ↑ A. V. Akimov, A. Mukherjee, C. L. Yu, D. E. Chang, A. S. Zibrov, P. R. Hemmer, H. Park, and M. D. Lukin. "Generation of single optical plasmons in metallic nanowires coupled to quantum dots. (http://www.fas.harvard.edu/~phys191r/References/d4/Akimov2007.pdf) ," Nature, 450:402–406, 15 November 2007.
29. ↑ B. Lounisa, H.A. Bechtela, D. Gerionc, P. Alivisatosc, and W.E. Moerner. "Photon antibunching in single cdse/zns quantum dot fluorescence (http://www.fas.harvard.edu/~phys191r/References/d4/Lounisa2000.pdf) ," Chemical Physics Letters, 329:399–404, October 2000.
30. ↑ T. Gaebel et al. "Room-temperature coherent coupling of single spins in diamond. (http://www.fas.harvard.edu/~phys191r/References/d4/Gaebel2006.pdf) ," Nature Physics, 2:408, 2006.
31. ↑ N.B. Manson, J.P. Harrison, and M.J. Sellars. "The nitrogen-vacancy center in diamond re-visited (http://www.fas.harvard.edu/~phys191r/References/d4/Manson2006.pdf) ," arXiv:cond-mat/0601360v2, 2006.
32. ↑ J. Wrachtrup and F. Jelezko. "Quantum information processing in diamond (http://www.fas.harvard.edu/~phys191r/References/d4/Wrachtrup2006.pdf) ." J. Phys.:Condens. Matter, 18:S807, 2006.
33. ↑ The model presented here is based on the recent theoretical work (Manson 2006), which provides an adequate explanation for most observations. According to this model, transitions between the triplet and singlet states occur via the spin-orbit interaction, which mixes states of the same irreducible representation. The excited state intersystem crossing favors the $m_s = \pm 1$ states because (in the absence of strain) there is an $A_1$ excited state with $S_x, S_y$ character. Conversely, the decay from the singlet leads to the $A_1$ ground state, which has spin projection $m_s = 0$.
34. ↑ A. Gruber et al. "Scanning confocal optical microscopy and magnetic resonance on single defect centers (http://www.fas.harvard.edu/~phys191r/References/d4/Gruber1997.pdf) ," Science, 276:2012, 1997.
35. ↑ E. van Oort, N.B. Manson, and M. Glasbeek. "Optically detected spin coherence of the diamond n-v centre in its triplet ground state (http://www.fas.harvard.edu/~phys191r/References/d4/vanOort1988.pdf) ," J. Phys. C: Solid State Phys., 21:4385, 1988.
36. ↑ E. van Oort, P. Stroomer, and M. Glasbeek. "Low-field optically detected magnetic resonance of a coupled triplet-doublet defect pair in diamond

(http://www.fas.harvard.edu/~phys191r/References/d4/vanOort1990.pdf) ," Phys. Rev. B, 42:8605, 1990.
37. ↑ A. Gruber et al. "Scanning confocal optical microscopy and magnetic resonance on single defect centers (http://www.fas.harvard.edu/~phys191r/References/d4/Gruber1997.pdf) ," Science, 276:2012, 1997.
38. ↑ N.B. Manson, J.P. Harrison, and M.J. Sellars. "The nitrogen-vacancy center in diamond re-visited (http://www.fas.harvard.edu/~phys191r/References/d4/Manson2006.pdf) ," arXiv:cond-mat/0601360v2, 2006.
39. ↑ L. Childress, J.M. Taylor, A.S. Sørensen, and M.D. Lukin. "Fault-tolerant quantum communication based on solid-state photon emitters (http://www.fas.harvard.edu/~phys191r/References/d4/Childress2006.pdf) ," Phys. Rev. Lett., 96:070504, 2006.
40. ↑ F. Jelezko et al. "Single spin states in a defect center resolved by optical spectroscopy (http://www.fas.harvard.edu/~phys191r/References/d4/Jelezko2002.pdf) ," App. Phys. Lett., 81:2160, 2002.
41. ↑ F.T. Charnock and T.A Kennedy. "Combined optical and microwave approach for performing quantum spin operations on the nitrogen-vacancy center in diamond (http://www.fas.harvard.edu/~phys191r/References/d4/Charnock2001.pdf) ," Phys. Rev. B, 64:041201(R), 2001.
42. ↑ X.F. He, N.B. Manson, and P.T.H. Fisk. "Paramagnetic resonance of photoexcited n-v defects in diamond. ii, hyperfine interaction with the n-14 nucleus (http://www.fas.harvard.edu/~phys191r/References/d4/He1993.pdf) ," Phys. Rev. B, 47:8816, 1993.
43. ↑ M. O. Scully and M. S. Zubairy. Quantum Optics. Cambridge University Press, Cambridge, UK, 1997.
44. ↑ M. O. Scully and M. S. Zubairy. Quantum Optics. Cambridge University Press, Cambridge, UK, 1997.
45. ↑ E.L. Hahn, “Spin Echoes (http://www.fas.harvard.edu/~phys191r/References/c4/hahn1950.pdf) ,” Phys. Rev. 80:580, 1950.
46. ↑ A. Schweiger and G. Jeschke. Principles of pulse electron paramagnetic resonance. Oxford University Press, Oxford, UK, 2001.

# Introductory reading

[1] "The Diamond Age of Spintronics (http://www.fas.harvard.edu/~phys191r/References/d4/Awschalom2007.pdf) ," David D. Awschalom, Ryan Epstein, and Ronald Hanson, Scientific American 297(4), 84 (October, 2007) is a very general introduction to the subject for non-specialists.

[2] Chapters 3 and 4 of Lillian Childress Ph.D. thesis contain a general overview of the subject and techniques (as of 2006), available online http://lukin.physics.harvard.edu/theses.htm

[3] Discussion of the level structure can be found in "Properties of nitrogen-vacancy centers in diamond: the group theoretic approach (http://www.fas.harvard.edu/~phys191r/References/d4/Maze2011.pdf) ," J. R. Maze, A. Gali, E. Togan, Y. Chu, A. Trifonov, E. Kaxiras and M. D. Lukin, New J. Phys. 13, 025025 (2011). See also Jeronimo Maze’s thesis http://lukin.physics.harvard.edu/theses.htm

# Bench notes

- National Instruments 6232 Multifunction ePCI card (http://www.fas.harvard.edu/~phys191r/Bench_Notes/D4/ni6323.pdf)
- National Instruments BNC-2090A Breakout Box

(http://www.fas.harvard.edu/~phys191r/Bench_Notes/D4/ni_bnc2090a.pdf)
- Dell Optiplex 980 Technical Guide (http://www.fas.harvard.edu/~phys191r/Bench_Notes/optiplex-980-tech-guide.pdf)
- Crystal Technology Acousto-Optic Modulator Principles of Operation (http://www.fas.harvard.edu/~phys191r/Bench_Notes/D4/AO_Modulator3000_appnote.pdf)
- Crystal Technology AOMO 3080-125 Acousto-Optic Modulator Spec Sheet (http://www.fas.harvard.edu/~phys191r/Bench_Notes/D4/AOM.pdf)
- Crystal Technology AODR 1080AF-DIF0-1.0 Acousto-Optic Modulator Driver (http://www.fas.harvard.edu/~phys191r/Bench_Notes/D4/AOM_driver.pdf)
- Crystal Technology AODR 1080AF-DIF0-1.0 Acousto-Optic Modulator Driver Test Sheet (http://www.fas.harvard.edu/~phys191r/Bench_Notes/D4/AOM_driver_test.pdf)
- Perkin Elmer SPCM-AQR-14-FC Single Photon Counting Module (http://www.fas.harvard.edu/~phys191r/Bench_Notes/D4/SPCMAQR.pdf)
- PicoQuant TimeHarp 200 PCI board for Time-Correlated Single Photon Counting (http://www.picoquant.com/products/timeharp200/timeharp200.htm)
- TimeHarp 200 Spec Sheet (pdf) (http://www.fas.harvard.edu/~phys191r/Bench_Notes/D4/TimeHarp200.pdf)
- TimeHarp 200 User Manual (large pdf) (http://www.fas.harvard.edu/~phys191r/Bench_Notes/D4/timeharp200_user.pdf)
- SpinCore Technologies PulseBlasterESR-PRO-400 PCI Pulse Generator Board (http://www.fas.harvard.edu/~phys191r/Bench_Notes/D4/PBESR-Pro_Manual.pdf)
- Nikon Objective Specifications (http://www.nikoninstruments.com/Products/Optics-Objectives/Fluor-Objectives/CFI-Plan-Fluor-Series/(specifications))
- Semrock LM01-552-25 dichroic filter (http://www.fas.harvard.edu/~phys191r/Bench_Notes/D4/semrockLM01-552-25.pdf)
- Omega Optical 3RD600LP long pass filter (http://www.fas.harvard.edu/~phys191r/Bench_Notes/D4/omega_3rd600lp.pdf)
- Newport 562-XYZ Translation Stage Interferometer Test Sheet (http://www.fas.harvard.edu/~phys191r/Bench_Notes/D4/newport_562xyz.pdf)
- Thorlabs FC632-50B-FC single mode 50/50 standard fused fiber optic coupler spec sheet (http://www.fas.harvard.edu/~phys191r/Bench_Notes/D4/Thorlabs_FC632_50B_FC.pdf)
- Thorlabs FC632-50B-FC single mode 50/50 standard fused fiber optic coupler test sheet (http://www.fas.harvard.edu/~phys191r/Bench_Notes/D4/Thorlabs_sm600_test.pdf)
- Thorlabs P1-630A-FC-2 single mode fiber patch cable (http://www.fas.harvard.edu/~phys191r/Bench_Notes/D4/Thorlabs_P1-630A-FC-2.pdf)
- Thorlabs F230FC-B Fiber Collimation Package (http://www.fas.harvard.edu/~phys191r/Bench_Notes/D4/Thorlabs_F230FC-B.pdf)
- Thorlabs MDT 693 Piezo Driver (http://www.fas.harvard.edu/~phys191r/Bench_Notes/D4/Thorlabs_mdt693a.pdf)
- Thorlabs Dual Axis Scanning Galvanometer Power Supply (http://www.fas.harvard.edu/~phys191r/Bench_Notes/D4/Thorlabs_gps011.pdf)
- Thorlabs Dual Axis Scanning Galvanometer System (http://www.fas.harvard.edu/~phys191r/Bench_Notes/D4/Thorlabs_gvs012.pdf)
- File:Nv electronics.pdf Block diagram of electronics (pdf)

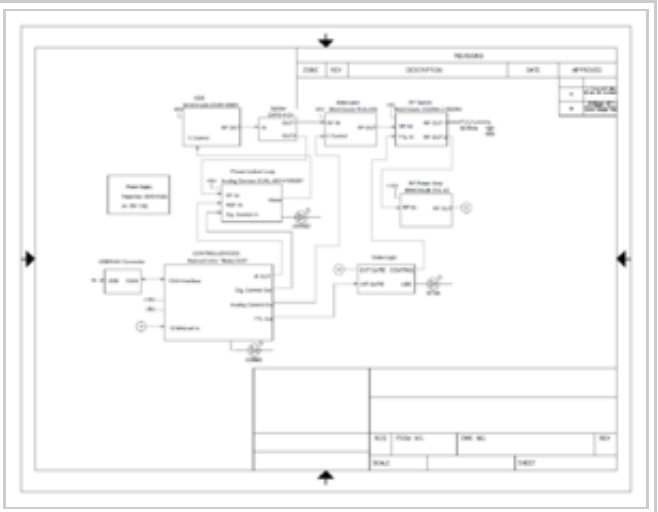

Block diagram of microwave source (png)

# Appendix: microwave source calibration

Evaluating MiniCircuits RVA33 attenuator -- two in series, with IFR spectrum analyzer, at 2.0 GHz, 0 dBm source.

Measured return signal with DUT replaced by SMA barrel is -3.58 dBm.

Measured return signal with DUT in place, powered with 5.0 V, various control voltages:

| Voltage (V) | Level (-dBm) |
|---|---|
| 0.0 | 80.94 |
| 0.1 | 83.72 |
| 0.2 | 83.58 |
| 0.3 | 83.94 |
| 0.4 | 83.91 |
| 0.5 | 83.75 |
| 0.6 | 83.22 |
| 0.7 | 81.20 |
| 0.8 | 71.94 |
| 0.9 | 54.36 |
| 1.0 | 42.08 |
| 1.1 | 35.50 |
| 1.2 | 31.13 |
| 1.3 | 28.34 |
| 1.4 | 26.24 |
| 1.5 | 24.69 |
| 1.6 | 23.56 |
| 1.7 | 22.66 |
| 1.8 | 21.88 |
| 1.9 | 21.18 |
| 2.0 | 20.55 |
| 2.1 | 20.11 |
| 2.2 | 19.61 |
| 2.3 | 19.15 |
| 2.4 | 18.77 |

| | |
|---|---|
| 2.5 | 18.38 |
| 2.6 | 18.03 |
| 2.7 | 17.63 |
| 2.8 | 17.27 |
| 2.9 | 16.94 |
| 3.0 | 16.58 |
| 3.1 | 16.20 |
| 3.2 | 15.84 |
| 3.3 | 15.48 |
| 3.4 | 15.11 |
| 3.5 | 14.81 |
| 3.6 | 14.45 |
| 3.7 | 14.09 |
| 3.8 | 13.72 |
| 3.9 | 13.33 |
| 4.0 | 12.91 |
| 4.1 | 12.66 |
| 4.2 | 12.19 |
| 4.3 | 11.86 |
| 4.4 | 11.44 |
| 4.5 | 11.10 |
| 4.6 | 10.69 |
| 4.7 | 10.20 |
| 4.8 | 9.83 |
| 4.9 | 9.50 |
| 5.0 | 9.15 |